Template revised September 2025

Title: Antibody efficacy in bacterial sepsis is rescued by targeting macrophage PAMP-STAT1-FcRn axis

Authors: Xinyu Wei[1,2]†, Xiaoxia Su[2]†, Qianyu Duan[1]†, Miao Pei[2], Qun Huang[1], Xuan Lai[1], Jiani Zhuang[1], Danzhi Wu[1], Beibei Chen[1], Yu Deng[1], Ying Huang[1], Jinzhou Ye[1], Teng Zhang[1], Hua Zhou[3], Xiaoting Hua[4,5], Xin Ding[6], Mao Li[2,7]*, Xianjie Liu[8]*, Wenjun Chen[9]*, Xinhai Chen[1,2,10]*

Affiliations:

[1]Insititute of Infectious Diseases, Shenzhen Bay Laboratory, Shenzhen 518132, China.

[2]Shenzhen Medical Academy of Research and Translation, Shenzhen 518107, China.

[3]Department of Respiratory and Critical Care Medicine, the Second Affiliated Hospital Zhejiang University, Hangzhou 310009, China.

[4]Department of Infectious Diseases, Sir Run Run Shaw Hospital, Zhejiang University School of Medicine, Hangzhou, 310016, China.

[5]Zhejiang Provincial Engineering Research Center of Innovative Instruments for Precise Pathogen Detection, Hangzhou, 310016, China.

[6]School of Medicine, Shenzhen Campus of Sun Yat-sen University, Shenzhen, 518107, China.

[7]Institute of Chemical Biology, Shenzhen Bay Laboratory, Shenzhen 518132, China.

[8]Shenzhen International Institute for Biomedical Research, Shenzhen 518116, China.

[9]Department of Laboratory Medicine, Third Affiliated Hospital of Sun Yat-Sen University, Tianhe Road 600#, Guangzhou 510630, China.

[10]Guangdong Provincial Key Laboratory of Infection Immunity and Inflammation, Shenzhen 518060, China.

***Corresponding author. Email: xinhaichen@szbl.ac.cn (X.C.); chenwj286@mail.sysu.edu.cn (W.C.); lxj309@163.com (X.L.).**

†These authors contributed equally to this work.

Abstract: Sepsis induces a significant loss of circulating IgG, but the underlying mechanism has remained obscure. Here, we identify a previously unrecognized pathogenic axis that directly links bacterial PAMPs to antibody failure. During bacterial sepsis, LPS and PGN potently activate macrophage STAT1, which in turn transcriptionally silences FcRn, collapsing IgG salvage pathways and driving rapid antibody catabolism. This IgG-destabilizing mechanism is strikingly macrophage-specific in the mouse liver and spleen and is conserved in human macrophages. Loss of macrophage FcRn ablates the antibody protection, whereas inhibition of Toll-like receptor 4 (TLR4) or STAT1 signaling potently enhances antibody efficacy in septic mice. These findings uncover a fundamental mechanism of sepsis-induced immunosuppression and reveal a tractable intervention point for rescuing antibody therapeutics against bacterial sepsis.

Main Text: Bacteremia often progresses to sepsis, a life-threatening condition characterized by dysregulated immune responses to invading pathogens. In septic patients, decreased IgG levels are consistently associated with increased mortality (*1-3*). Although this correlation is well-established, the mechanism underlying IgG reduction remains elusive. Several hypotheses have been proposed, including antigen-driven consumption, extravasation resulting from increased vascular permeability, B cell dysfunction, and accelerated catabolism (*4-6*). However, the relative contributions of these processes remain poorly defined, and the potential involvement of other, unrecognized mechanisms cannot be ruled out. Elucidating these mechanisms are therefore critical for developing novel therapeutic strategies for bacterial sepsis.

Driven by the antibiotic resistance crisis, antibody therapies have been developed for bacterial sepsis, yet the majority of their clinical trials have failed for reasons that are still poorly understood (*7, 8*). The observed reduction in endogenous IgG levels during sepsis raises the possibility that a parallel reduction may occur in the circulating concentrations of exogenously administered therapeutic antibodies. This could explain the inconsistent clinical outcomes reported with intravenous immunoglobulin (IVIG) in septic patients (*5, 9*). If a general mechanism driving IgG reduction exists, it also likely compromises the pharmacokinetics of pathogen-specific antibodies, preventing them from reaching and maintaining therapeutic levels. This may account for the heterogeneous efficacy observed in clinical evaluations of those antibody therapies.

IgG antibodies can clear bacterial infections via FcγR- and complement receptor (CR)-mediated phagocytosis, leading to lysosomal degradation of both the antibodies and engulfed pathogens (*10, 11*). In parallel, the neonatal Fc receptor (FcRn) critically influences IgG homeostasis by orchestrating a salvage pathway that recycles IgG from lysosomal degradation, thereby ensuring its prolonged circulating half-life (*12*). At present, it remains unclear whether sepsis alters the function of these receptors and whether such impairment ultimately contributes to a characteristic decline in circulating antibody levels. Defining the dominant mechanism and identifying key therapeutic targets are crucial for rescuing antibody efficacy in sepsis.

Results

Mouse sepsis recapitulates circulating IgG loss observed in patients

Profiling of patients with bacterial sepsis stratified by survival outcome revealed a striking divergence in endogenous IgG kinetics (Fig. 1A). Specifically, survivors exhibited a fluctuating rise in IgG levels over time, in contrast to the overall stagnation or decline observed in non-survivors, a finding with significant prognostic implications. Intriguingly, a similar decline in endogenous total IgG levels was also observed in mouse models of sepsis induced by bloodstream infection with either pathogenic *Escherichia coli* (Gram-negative bacterium) or a *Staphylococcus aureus* (Gram-positive bacterium) strain deficient in *spa*, *sbi*, and *ssl10* genes (Fig. 1B; fig. S1, A and B). These genes encode immunoglobulin-binding proteins previously shown in our work to mediate circulating IgG loss (*13*), a process that could confound the sepsis-specific phenotype under investigation. While endogenous total IgM levels also decreased in these mouse sepsis models (Fig. 1C), administration of intravenous immunoglobulin (IVIG), which contains both human IgG (hIgG) and IgM (hIgM), revealed a critical divergence in clearance kinetics between IgG and IgM (Fig. 1, D and E). Specifically, bacterial sepsis markedly accelerated the clearance of hIgG but left hIgM clearance unchanged. To substantiate this finding, we tracked the clearance of exogenous IgG monoclonal antibodies (mAbs) that were

not specific to the infecting pathogens (Fig. 1, F-J). These included a hIgG1 administered to both wild-type (WT) and mature B cell-deficient (DKO) mice, a long-acting hIgG1 variant with YTE mutations (*14, 15*) evaluated in human FcRn (hFcRn) transgenic mice, and a mouse IgG2b (mIgG2b). All of these exogenous IgG forms exhibited more rapid decline during sepsis (Fig. 1, F-J). In contrast, a mIgM mAb recognizing the same antigen as the mIgG2b did not show accelerated clearance (Fig. 1K). This dissociation suggests that distinct mechanisms underlie the loss of endogenous IgG versus IgM, with the former potentially sharing a common pathway with accelerated clearance of exogenous IgG.

To determine the mechanism underlying this accelerated IgG clearance, we first investigated whether it could be attributed to enhanced tissue distribution or fecal excretion. However, the hIgG1 levels in both perfused and non-perfused tissues, as well as fecal samples, did not differ significantly between septic and control mice (Fig. 1, L-N). Furthermore, the clearance mechanism was independent of antigen recognition. This was evidenced by the fact that the IVIG preparation contained negligible pathogen-specific antibodies (fig. S1, C and D), all administered mAbs were non-binding to the pathogens used (fig. S1, E and F), and no anti-*E. coli* or anti-*S. aureus* antibodies were detectable in the serum of septic mice during the experimental timeframe (fig. S1, G-J). Together, these results strongly support that bacterial sepsis drives the loss of both endogenous and exogenous IgG in mice through a mechanism consistent with non-antigen-specific consumption.

Macrophage FcRn reduction mediates circulating IgG loss in septic mice

Having ruled out non-specific consumption, we hypothesized that the accelerated IgG clearance was mediated by receptors governing IgG homeostasis. To this end, we primarily profiled the expression of FcγRs, CRs, and FcRn in immune cells from septic mice, including neutrophils, monocytes, and macrophages in both circulation and tissues, by flow cytometry. However, our screening revealed that the expression changes of individual FcγRs and CRs lacked a consistent or unified trend between the *E. coli* and *S. aureus* sepsis models (fig. S2), arguing against their primary role in the observed IgG loss. Strikingly, we discovered a convergent downregulation of FcRn in liver and splenic macrophages across both bacterial sepsis models (Fig. 2, A and B; fig. S3A), which was further confirmed at the transcriptional level (fig. S3B), although the abundance of hepatic macrophages (Kupffer cells) was not markedly reduced (fig. S3, C and D). Given the established role of endothelial FcRn in IgG homeostasis (*12*), we extended our analysis to liver and lung endothelial cells. Although we observed a moderate reduction in endothelial cell numbers in liver (fig. S3, E-H), FcRn expression in these cells was not significantly altered (Fig. 2, A and B). To establish a direct causal link, we employed an *in vitro* model using bone marrow-derived macrophages (BMDMs). Bacterial challenge recapitulated the *in vivo* findings, inducing significant downregulation of FcRn at both the protein and transcriptional levels (Fig. 2, C and D). To determine if the observed FcRn downregulation directly mediates circulating IgG loss, we subjected *Fcgrt*$^{-/-}$ mice to our established bacterial sepsis models (fig. S3, I and J). Upon infection with either pathogenic *E. coli* or *S. aureus*, both WT and *Fcgrt*$^{-/-}$ mice exhibited comparable body weight loss and bacterial loads across tissues (fig. S3, K-N), indicating a similar disease severity. Strikingly, unlike in WT mice, endogenous IgG levels in *Fcgrt*$^{-/-}$ mice did not decline significantly in response to sepsis (Fig. 2E and 1B). Similarly, the clearance of administered hIgG1 was not accelerated in septic *Fcgrt*$^{-/-}$ mice compared to their non-septic counterparts (Fig. 2F and 1F). To further define the role of macrophage FcRn, we generated mice with a myeloid-specific knockout of *Fcgrt* (*Fcgrt*$^{f/f}$ *LysM-Cre*). Bacterial sepsis induced by either pathogen resulted in body weight loss and tissue

bacterial loads that were indistinguishable between *Fcgrt*$^{f/f}$ and *Fcgrt*$^{f/f}$ *LysM-Cre* mice (Fig. 2, G-I), ruling out confounding differences in infection dynamics. Notably, the accelerated IgG clearance found in septic *Fcgrt*$^{f/f}$ controls was absent in septic *Fcgrt*$^{f/f}$ *LysM-Cre* mice (Fig. 2, J and K), indicating that the sepsis-induced downregulation of FcRn in macrophages is a primary driver of the circulating IgG decline.

LPS and PGN reduce macrophage FcRn, leading to circulating IgG loss

We next asked which bacterial components trigger the FcRn-dependent IgG loss. Given the established role of LPS as a key mediator in sepsis, we first employed toll-like receptor 4 (TLR4)-deficient mice subjected to pathogenic *E. coli*-induced sepsis. The accelerated decline in hIgG1 levels observed in TLR4$^{+/+}$ control mice was absent in TLR4$^{-/-}$ mice (Fig. 3A), despite equivalent disease severity as measured by body weight loss and tissue bacterial loads (fig. S4, A and B), indicating that the phenotype was not attributable to differences in infection outcome. Since LPS is essential in *E. coli*, we utilized *Acinetobacter baumannii*, employing both WT and an LPS-deficient mutant strain with a IS*Aba1* insertion in *lpxC* (*16*) (Fig. 3, B and C). Although LPS loss markedly attenuates virulence (*17*), to compensate for this, we administered a threefold higher inoculum of the mutant strain. This achieved comparable bacterial loads across tissues between mutant- and WT-infected mice at 6-24 hours post-infection (fig. S4C). Using this model, we found that only WT *A. baumannii* infection reduced endogenous IgG levels and accelerated the clearance of exogenous hIgG1 (Fig. 3, B and C). Despite similar bacterial loads during early infection, the LPS-deficient mutant did not recapitulate the IgG loss phenotype (Fig. 3, B and C), demonstrating that LPS is the principal factor mediating circulating IgG loss in Gram-negative bacteria-induced sepsis. Accordingly, administration of exogenous LPS nearly phenocopied the loss of both endogenous IgG and various exogenous IgG mAbs observed in pathogenic *E. coli* infection (Fig. 3, D-F; Fig. 1, B, F, G, and I), and this effect was also abolished in TLR4$^{-/-}$ mice (Fig. 3G). Similarly, administration of peptidoglycan (PGN) from *S. aureus* induced an acceleration of hIgG1 clearance comparable to that detected in LPS-treated mice (Fig. 3D).

The observed circulating IgG loss mediated by LPS or PGN prompted us to investigate their effect on FcRn expression. *In vivo*, both LPS and PGN selectively downregulated FcRn at the protein and transcriptional levels in splenic and hepatic macrophages (Fig. 3, H and I; fig. S4F), without affecting other tested cells (fig. S4, D and E). The decline in FcRn in splenic macrophages was accompanied by elevated cytokine expression (fig. S4, G and H). This FcRn downregulation was also replicated in BMDMs but not in human umbilical vein endothelial cells (HUVECs) (Fig. 3, J and K; fig. S4, I-K), where robust cytokine induction confirmed effective LPS or PGN treatment (fig. S4, L-N). FcRn deficiency had no impact on the phagocytic capacity of BMDMs with or without LPS stimulation (Fig. 3L). However, intracellular levels of hIgG1 were substantially lower in *Fcgrt*$^{-/-}$ BMDM compared to WT controls (Fig. 3M), indicating rapid IgG degradation in the absence of FcRn. Moreover, LPS and PGN stimulation markedly reduced hIgG1 levels in WT BMDMs (Fig. 3, M and N), directly linking PAMP-induced FcRn downregulation to impaired IgG transcytosis and enhanced intracellular IgG degradation in macrophages. As expected, neither LPS nor PGN alone accelerated the clearance of exogenous hIgG1 in *Fcgrt*$^{-/-}$ mice (Fig. 3, O and P). Collectively, these results indicate that specific bacterial PAMPs, notably LPS and PGN, serve as critical bacterial factors in sepsis-induced circulating IgG loss, operating through selective downregulation of FcRn in macrophages and consequent disruption of IgG homeostasis.

STAT1 activation impairs macrophage FcRn expression in sepsis

We further asked how specific PAMPs during bacterial sepsis reduced FcRn expression in macrophages. Given that LPS or PGN treatment in BMDMs recapitulated the FcRn reduction observed in splenic and liver macrophages during bacterial sepsis (Fig. 2, A and B; Fig. 3, J and K), we first investigated whether NF-κB mediated this reduction in this model. Although NF-κB is a well-known sepsis-related transcription factor, its inhibition unexpectedly further decreased FcRn expression in LPS- or PGN-treated BMDMs (Fig. 4A), even though it effectively suppressing cytokine expression (fig. S5, A and B). This indicates that NF-κB activation indeed exerts a protective effect on FcRn expression. We next examined the role of type I interferon in FcRn reduction following observations of its robust induction in PAMP- or bacteria-treated macrophages (*18*) (fig. S5B and S4H). However, in BMDMs from A129 mice (*Ifnar1* knockout), LPS stimulation, while still inducing robust expression of cytokines (fig. S5, C and D), failed to restore FcRn expression (Fig. 4B). Moreover, both bacterial sepsis and LPS administration still accelerated the clearance of hIgG1 in A129 mice (Fig. 4, C and D), mirroring the trend observed in WT mice (Fig. 1F and 3D). A129 mice also exhibited a susceptibility to bacterial sepsis comparable to that of WT mice (fig. S5E). These results indicate that type I interferon is not required for FcRn reduction during sepsis.

To uncover the mechanism underlying FcRn reduction, we performed bulk RNA-seq on Kupffer cells and splenic macrophages isolated from septic mice. Principal component analysis revealed a clear separation between the transcriptomic profiles of Kupffer cells and splenic macrophages from healthy mice and those with bacterial sepsis (Fig. 4E). This transcriptomic data further confirmed that FcRn expression was significantly reduced in both Kupffer cells and splenic macrophages of septic mice (fig. S5F). A total of 503 genes were commonly differentially expressed in these two macrophage populations following bacterial sepsis (Fig. 4F). Using these shared differentially expressed genes for transcription factor (TF) activity inference, we identified 11 TFs whose activities were significantly and concordantly regulated in both Kupffer cells and splenic macrophages during bacterial sepsis (Fig. 4, G and H). Interestingly, two of these TFs, *Stat1* and *Spi1*, were also identified in the public macrophage cistrome data (The Signaling Pathways Project) as potential direct regulators of the *Fcgrt* locus (Fig. 4H). Treatment with the STAT1 inhibitor fludarabine but not PU.1 (encoded by *Spi1*) inhibitor DB2313 rescued FcRn expression in LPS- or PGN-stimulated BMDMs without suppressing the expression of cytokines (Fig. 4I, fig. S5, G-I). STAT1 has been implicated as a negative regulator for FcRn in response to type II interferon (IFN-γ) *in vitro* (*19*); however, its role in regulating FcRn expression during bacterial sepsis remains unclear. We confirmed that bacterial infections or PAMP stimulations markedly induced STAT1 phosphorylation at both tyrosine 701 and serine 727 residues in BMDMs, while failing to trigger IFN-γ expression (Fig. 4J; fig. S5, J and K). To validate this *in vivo*, the $stat1^{-/-}$ mice were chosen. Since $stat1^{+/+}$ and $stat1^{+/-}$ showed a similar trend of accelerated hIgG1 clearance (fig. S5L), we randomly selected one of these two genotypes to serve as the control group in subsequent studies. The $stat1^{-/-}$ mice did not exhibit increased susceptibility to bacterial sepsis, as evidenced by comparable body weight loss and tissue bacterial loads to controls (fig. S5, M-O). Strikingly, genetic deletion of *stat1* profoundly rescued FcRn reduction in liver macrophages and significantly, albeit partially, restored FcRn expression in splenic macrophages following bacterial sepsis (Fig. 4, K-N). Consequently, the bacterial sepsis-induced loss of circulating hIgG1 was also significantly ameliorated in $stat1^{-/-}$ mice (Fig. 4, O and P). Thus, these data establish STAT1 activation as a pathophysiological promoter of FcRn reduction and resultant circulating IgG loss during bacterial sepsis.

Bacterial infections disrupt IgG transcytosis in human macrophages

We established that in murine bacterial sepsis, a specific PAMP-STAT1-FcRn axis is triggered, wherein PAMP activate STAT1, leading to FcRn suppression in macrophages and the consequent loss of circulating IgG. This discovery prompted us to investigate the translational relevance of this axis in human sepsis. We began by interrogating public datasets to determine whether *Fcgrt* expression is altered in septic patients. Re-analysis of two independent cohorts confirmed that *Fcgrt* expression was significantly downregulated in whole blood or peripheral leukocytes from septic patients compared to healthy controls (Fig. 5A and fig. S6A). In the GSE65682 dataset, Kaplan-Meier survival analysis with the log-rank test revealed that septic patients with higher *Fcgrt* expression had a greater probability of survival relative to those with lower expression (Fig. 5B). Re-analysis of GSE63042 dataset showed that sepsis survivors exhibited elevated *Fcgrt* levels in whole blood and contained a higher proportion of individuals with high *Fcgrt* expression compared to sepsis non-survivors (Fig. 5, C and D). To validate these findings, we collected blood samples from septic patients and healthy donors. Our analysis of $CD14^+$ monocytes from these samples revealed a significant reduction in FcRn expression in patients (Fig. 5E). We next infected $CD14^+$ monocyte-derived macrophages (hMDMs) with *E. coli* or *S. aureus* and found that this infection triggered a time- and dose-dependent suppression of FcRn expression (Fig. 5, F and G; fig. S6, B and C), a result that consistent with reanalyzed data from public datasets on PBMCs or human macrophages (fig. S6, D and E). Furthermore, our experiments established that LPS or PGN stimulation was sufficient to significantly downregulate FcRn in $CD14^+$ hMDMs (Fig. 5, H and I), an effect we also confirmed in $CD14^+$ monocytes following PAMP challenge (fig. S6, F-J).

We next examined STAT1 signaling pathway. In $CD14^+$ hMDMs, both bacterial infection and PAMP stimulation promptly induced phosphorylation of STAT1 at Ser727 and Tyr701 (Fig. 5, J and K). These phosphorylation events occurred early after exposure, aligning with previous observations in mouse BMDMs (Fig. 4J). The inhibition of STAT1 phosphorylation at Tyr701 (by Ruxolitinib, RUX) or at Ser727 (by Adezmapimod, ADE) in hMDMs rescued the downregulation of FcRn expression induced by LPS or PGN (Fig. 5, L and M), demonstrating STAT1-dependent regulation of FcRn. PAMP stimulation did not reduce the phagocytic capacity of hMDMs (Fig. 5N) but instead reduced their hIgG1 transcytosis (Fig. 5O). Hence, our data demonstrate that in human macrophages, bacteria and their PAMPs activate STAT1 to suppress FcRn, thereby impairing IgG transcytosis. This confirms that the PAMP-STAT1-FcRn axis, first identified in mouse sepsis, is conserved in humans.

Targeting PAMP-STAT1-FcRn axis rescues antibody efficacy in bacterial sepsis

The therapeutic efficacy of antibodies is known to correlate positively with concentration within a defined therapeutic range. Our data are consistent with this principle that IVIG protects against *E. coli* and *S. aureus* sepsis in a clear dose-dependent manner (fig. S7, A and B). To determine whether IVIG efficacy depends on macrophage FcRn expression, we compared outcomes in $Fcgrt^{f/f}$ and $Fcgrt^{f/f}$ LysM-Cre mice during bacterial sepsis. While macrophage-specific FcRn deletion did not alter host susceptibility to either *E. coli* or *S. aureus* sepsis, it completely abrogated the protective effect of IVIG (Fig. 6, A and B). Specifically, IVIG significantly improved survival in $Fcgrt^{f/f}$ mice but failed to protect $Fcgrt^{f/f}$ LysM-Cre mice (Fig. 6, A and B), indicating that the loss of IVIG efficacy upon macrophage FcRn deletion is attributable to impaired antibody persistence *in vivo*. Next, we asked whether therapeutic targeting of the PAMP-STAT1-FcRn axis could enhance antibody-mediated protection against bacterial sepsis. Notably, genetic ablation of STAT1 did not affect survival in *E. coli* sepsis but slightly increased tolerance to *S. aureus* infection (Fig. 6, C and D). More importantly, IVIG-mediated protection

was significantly augmented in *STAT1*$^{-/-}$ mice against both pathogens compared to *STAT1*$^{+/-}$ controls (Fig. 6, C and D). Pharmacologic inhibition of STAT1 with carnosic acid (CA) similarly improved IVIG efficacy (Fig. 6E), confirming that dampening STAT1 activity improves antibody-based intervention outcomes in bacterial sepsis. We extended these findings to a pathogen-specific mAb, 3E9, which targets the conserved O25b LPS antigen of *E. coli* ST131 lineage (*20*). Although 3E9 exhibited strong binding to *E. coli* used in this study (fig. S7C), its low dose provided no protection in WT mice during *E. coli* sepsis (Fig. 6F). In contrast, its efficacy was markedly enhanced in TLR4-deficient mice (Fig. 6F), accompanied by significantly improved serum 3E9 persistence compared to septic *TLR4*$^{+/+}$ controls (Fig. 6G). Consistently, 3E9 improved survival in *Fcgrt*$^{f/f}$ mice but failed to protect *Fcgrt*$^{f/f}$ LysM-Cre mice (Fig. 6H). Furthermore, 3E9 conferred protection in *STAT1*$^{-/-}$ but not *STAT1*$^{+/-}$ mice (Fig. 6I). These results demonstrate that bypassing PAMP-triggered signaling rescues sepsis-induced antibody failure, thereby defining the therapeutic potential of modulating the PAMP-STAT1-FcRn axis to enhance antibody efficacy.

Discussion

Antibodies are essential for defense against bacterial infections, a function that depends on sustained IgG levels to enable rapid responses to pathogenic challenge. However, bacterial sepsis disrupts this fundamental requirement. We found that bacterial sepsis subverts this defense by reducing both endogenous and exogenous IgG in mice, mirroring the clinical observation of decreased circulating IgG in septic patients, where higher levels are associated with improved survival (*1-4, 21*). Mechanistically, this IgG loss was uncoupled from an antigen-specific immune response, tissue redistribution, or fecal excretion, and was instead mediated by the PAMP-STAT1-FcRn axis in macrophages. During sepsis, bacterial components such as LPS and PGN activated STAT1 signaling, leading to suppressed FcRn expression, impaired IgG recycling, and consequently, lowered circulating IgG. Crucially, intervention against key components of this axis rescued antibody-mediated protection against bacterial sepsis. Our work thus defines the PAMP-STAT1-FcRn axis as a central mechanism driving antibody loss in bacterial sepsis, providing a conceptual framework and proof-of-principle for targeting this pathway to rescue antibody immunity in septic patients.

While FcRn is widely expressed, its role in maintaining IgG levels is primarily mediated by endothelial cells, macrophages, and monocytes (*12, 22*). In murine bacterial sepsis, we found that FcRn was specifically downregulated in hepatic and splenic macrophages, which represent over 35% of the total macrophage population (*23*), while its expression remained unchanged in monocytes and endothelial cells. Importantly, bacterial infection induced a pronounced reduction in liver endothelial cell numbers while sparing the macrophage population; yet, IgG transcytosis was specifically suppressed in macrophages. Since macrophages primarily degrade IgG when FcRn is compromised (*24*), our observations reveal a critical functional dilemma wherein macrophages face an increased burden of IgG salvage due to the loss of endothelial cells, but simultaneously, their capacity to perform this task is compromised by FcRn downregulation, thereby resulting in IgG hypercatabolism. Thus, FcRn downregulation in splenic and hepatic macrophages constitutes a key mechanism underlying sepsis-induced circulating IgG loss, as evidenced by the fact that *Fcgrt*$^{f/f}$ *LysM-Cre* mice with bacterial sepsis exhibited equivalent levels of IgG loss as those without infection, thereby establishing the central role of macrophages and revealing a previously unrecognized pathogen-induced antibody evasion strategy via FcRn reprogramming.

Although significant interest has focused on FcRn-based therapeutic strategies, the regulation of its expression remains far less explored. If FcRn expression is compromised during infection, then engineering antibody-FcRn affinity alone may be insufficient to achieve the desired therapeutic outcomes. Several viruses have been reported to hijack FcRn. Enterovirus B and human astrovirus utilize FcRn as a functional receptor to facilitate viral replication (*25-27*). Human cytomegalovirus employs the US11 protein to bind FcRn and promote its ubiquitin-mediated degradation (*28*). Herpes simplex virus-1 infection upregulates DNA methylation at the FCGRT locus to suppress FcRn expression (*29*). In contrast, how bacterial infection regulates host FcRn expression has remained largely undefined. This study identifies that in bacterial sepsis, bacterial LPS and PGN downregulate macrophage FcRn through STAT1 activation. Unlike the previously reported IFN-γ-dependent STAT1-FcRn pathway observed *in vitro* (*19*), the current findings establish that LPS and PGN directly activate STAT1 in macrophages without substantial IFN-γ induction. This FcRn suppression exhibited striking tissue specificity, occurring specifically in hepatic and splenic macrophages. Thus, our finding, taken together with established tissue-specific methylation patterns at the FCGRT locus (*30*), suggests distinct regulatory mechanisms for FcRn expression in macrophages, monocytes, and endothelial cells across different tissues. The discovery of the PAMP-STAT1-FcRn axis provides a compelling rationale for this paradigm, underscoring the critical need to understand pathologic regulation of FcRn for future therapeutic development.

Current management of bacterial sepsis remains centered on infection control and supportive care (*31*). Antibody-based therapeutic strategies have long attracted significant attention for their potential to improve outcomes, but none have yet achieved clinical success (*32-34*). Such strategies encompass agents ranging from IVIG to mAbs targeting host factors like CD14 or TNFα or specific pathogen-derived antigens. Nevertheless, several antibody-based agents continue to be evaluated in active clinical trials, with many focusing on modulation of host immune responses (*35-37*). This collective effort suggests that immunomodulation may offer wide-ranging benefits in septic patients (*38, 39*). To explore this potential, our research has identified a highly conserved PAMP-STAT1-FcRn axis, a new immunoregulatory pathway, in human macrophages and monocytes. Published data together with our clinical observations further demonstrate that elevated FcRn expression in these immune cells correlates positively with improved clinical outcomes in bacterial sepsis. These findings suggest that targeting the PAMP-STAT1-FcRn axis could enhance the efficacy of antibody-based therapies. Preclinically, various interventions along this pathway, such as TLR4 knockout and STAT1 deletion or functional inhibition, consistently improved the protective efficacy of both IVIG and the anti-*E. coli* mAb 3E9 (*20*) in septic models, whereas macrophage-specific *Fcgrt* knockout abolished that protection. A future refined strategy would be to deliver FcRn mRNA via lipid-based nanoparticles or macrophage-derived exosomes (*40-42*), thereby enhancing FcRn expression in macrophages and boosting antibody efficacy. Collectively, our work supports the idea that modulating the PAMP-STAT1-FcRn axis may not only potentiate new antibody therapeutics but also restore previously ineffective candidates in bacterial sepsis, offering a new pathway toward clinical relevance for targeted immunomodulation.

Materials and Methods summary

Full details are available in the supplementary materials.

Ethnic statement

The Shenzhen Bay Laboratory Medical Ethical Committee reviewed, approved, and supervised the protocol (No. YL 2024-017) used for all experiments utilizing blood from human volunteers and informed consent forms were obtained from all participants. Animal research was performed in accordance with institutional guidelines following experimental protocol review, approval, and supervision by the Institutional Animal Care and Use Committee at the Shenzhen Bay Laboratory (Approval No. AECXH202201). Experiments with pathogenic *Escherichia coli*, *Staphylococcus aureus*, and *Acinetobacter baumannii* were performed in biosafety level 2 (BSL2)/animal BSL2 (ABSL2) containment upon review by Shenzhen Bay Laboratory Institutional Biosafety Committee.

Bacteria

The *S. aureus* Δ*spa*Δ*sbi*Δ*ssl10* mutant used in this study is maintained in our laboratory and was originally provided by Dr. Dominique Missiakas (The University of Chicago). The pathogenic *E. coli* BSI099 strain was a kind gift from Dr. Guobao Tian (Sun Yat-sen University), and the isogenic *lpxC* mutant was previously constructed in the *A. baumannii* ATCC 17978 background (*16*). For routine culture, *S. aureus* was grown in tryptic soy broth (TSB) or on TSB agar, while both *E. coli* and *A. baumannii* were cultivated in Luria broth (LB) or on LB agar; all strains were incubated at 37°C.

Mouse sepsis model

A monomicrobial murine sepsis model was generated using *S. aureus*, *E. coli*, or *A. baumannii*. Briefly, *S. aureus* cultures were grown to OD_{600} 0.45 and *E. coli* and *A. baumannii* to OD_{600} 1.0, pelleted, washed once in PBS, and resuspended to the desired CFU/ml. Mice received 100 µl of inoculum via the retro-orbital plexus (*S. aureus*, *E. coli*) or intraperitoneally (*A. baumannii*) under anesthesia. Animals were monitored daily for clinical signs and weight loss. At predefined time points, serum and liver, kidney, and spleen samples were collected. Serum Ig levels were quantified, and tissues were weighed, homogenized, diluted, and plated to determine bacterial burdens (CFU/g). Survival was recorded to assess antibody efficacy.

Antibody concentration assay

Serum and tissue antibody levels were quantified by ELISA using anti-human or anti-mouse Ig capture and HRP-conjugated detection antibodies. Human and mouse IgG/IgM, as well as exogenously administered antibodies, were measured on antigen- or isotype-specific plates and quantified against standard curves. Human IgM was measured using a commercial ELISA kit.

Flow cytometric analysis

Single-cell suspensions from mouse spleen, liver, and lung were prepared by enzymatic and/or mechanical dissociation followed by RBC lysis. Cells were stained with viability dye, lineage and myeloid markers, FcγR antibodies, and intracellular FcRn antibody after fixation/permeabilization. Major immune and endothelial populations were gated using standard markers, and data were acquired on a CytoFLEX LX cytometer.

Bone marrow–derived macrophages (BMDMs)

Mouse bone marrow cells were differentiated into macrophages for 7 days in M-CSF-containing medium. BMDMs were stimulated with bacteria, LPS, or PGN, with or without inhibitor pretreatment. Cells (>95% CD11b+F4/80+) were analyzed for FcRn expression by intracellular staining following fixation and permeabilization.

Isolation and differentiation of primary human monocytes

PBMCs from healthy donors or septic patients were isolated by density centrifugation, and $CD14^+$ monocytes were purified magnetically and differentiated into macrophages with M-CSF. Human macrophages or PBMCs were stimulated with LPS, PGN, or bacteria, with optional inhibitor pretreatment. Surface and intracellular markers, including FcRn, were assessed by flow cytometry in viable $CD11b^+CD14^+$ monocyte/macrophage populations.

Public dataset analysis

The prognostic significance of *Fcgrt* expression was evaluated using GEO cohorts. In GSE65682, an optimal cutoff for *Fcgrt* was derived using the *maxstat* algorithm to stratify patients for Kaplan-Meier survival analysis. Findings were independently validated in GSE63042 using median dichotomization. Additional datasets (GSE28750, GSE33341) were used to compare *Fcgrt* expression between sepsis and healthy controls, and GSE13670 was analyzed to assess *Fcgrt* induction in human macrophages following *S. aureus* infection.

Evaluation of antibody protection in mice

The protective effects of IVIG, the 3E9 monoclonal antibody, and STAT1 inhibitors were tested in murine monomicrobial sepsis. Antibodies were administered intraperitoneally before bacterial challenge, and inhibitors were given twice daily for 3 days starting 2 h before infection. Mice were infected intravenously with *S. aureus* Δ*spa*Δ*sbi*Δ*ssl10* or *E. coli* BSI099, and survival was monitored throughout the study.

Statistical analysis

Data were analyzed using GraphPad Prism with appropriate parametric tests, including two-tailed Student's *t* test, one-way or two-way ANOVA with multiple-comparison corrections, and log-rank tests for survival curves. Results are shown as mean ± SEM, with significance defined as $P < 0.05$.

References and Notes

1. J. F. Bermejo‐Martín *et al.*, Immunoglobulins IgG1, IgM and IgA: a synergistic team influencing survival in sepsis. *Journal of Internal Medicine* **276**, 404–412 (2014).
2. M. Akatsuka, H. Tatsumi, T. Sonoda, Y. Masuda, Low immunoglobulin G level is associated with poor outcomes in patients with sepsis and septic shock. *Journal of Microbiology, Immunology and Infection* **54**, 728–732 (2021).
3. F. S. Taccone, P. Stordeur, D. De Backer, J. Creteur, J.-L. Vincent, γ-Globulin Levels in Patients with Community-Acquired Septic Shock. *Shock* **32**, 379–385 (2009).
4. F. Venet *et al.*, Assessment of plasmatic immunoglobulin G, A and M levels in septic shock patients. *International Immunopharmacology* **11**, 2086–2090 (2011).
5. M. Akatsuka, Y. Masuda, H. Tatsumi, T. Sonoda, Efficacy of Intravenous Immunoglobulin Therapy for Patients With Sepsis and Low Immunoglobulin G Levels: A Single-Center Retrospective Study. *Clinical Therapeutics* **44**, 295–303 (2022).
6. C. Schmidt, S. Weißmüller, C. C. Heinz, Multifaceted Tissue-Protective Functions of Polyvalent Immunoglobulin Preparations in Severe Infections—Interactions with Neutrophils, Complement, and Coagulation Pathways. *Biomedicines* **11**, (2023).
7. X. Chen, D. Missiakas, Novel Antibody-Based Protection/Therapeutics in Staphylococcus aureus. *Annual Review of Microbiology* **78**, 425–446 (2024).

8. H. Wang, D. Chen, H. Lu, Anti-bacterial monoclonal antibodies: next generation therapy against superbugs. *Applied Microbiology and Biotechnology* **106**, 3957–3972 (2022).
9. T. Tagami, H. Matsui, K. Fushimi, H. Yasunaga, Intravenous Immunoglobulin and Mortality in Pneumonia Patients With Septic Shock: An Observational Nationwide Study. *Clinical Infectious Diseases* **61**, 385–392 (2015).
10. F. Nimmerjahn, J. V. Ravetch, Fcγ receptors as regulators of immune responses. *Nature Reviews Immunology* **8**, 34–47 (2008).
11. G. Delidakis, J. E. Kim, K. George, G. Georgiou, Improving Antibody Therapeutics by Manipulating the Fc Domain: Immunological and Structural Considerations. *Annual Review of Biomedical Engineering* **24**, 249–274 (2022).
12. M. Pyzik, L. K. Kozicky, A. K. Gandhi, R. S. Blumberg, The therapeutic age of the neonatal Fc receptor. *Nature Reviews Immunology* **23**, 415–432 (2023).
13. X. Chen, O. Schneewind, D. Missiakas, Engineered human antibodies for the opsonization and killing ofStaphylococcus aureus. *Proceedings of the National Academy of Sciences* **119**, (2022).
14. W. F. Dall'Acqua, P. A. Kiener, H. Wu, Properties of Human IgG1s Engineered for Enhanced Binding to the Neonatal Fc Receptor (FcRn). *Journal of Biological Chemistry* **281**, 23514–23524 (2006).
15. J. B. Domachowske *et al.*, Safety, Tolerability and Pharmacokinetics of MEDI8897, an Extended Half-life Single-dose Respiratory Syncytial Virus Prefusion F-targeting Monoclonal Antibody Administered as a Single Dose to Healthy Preterm Infants. *Pediatric Infectious Disease Journal* **37**, 886–892 (2018).
16. X. Mu *et al.*, The Effect of Colistin Resistance-Associated Mutations on the Fitness of Acinetobacter baumannii. *Frontiers in Microbiology* **7**, (2016).
17. K. Novović, B. Jovčić, Colistin Resistance in Acinetobacter baumannii: Molecular Mechanisms and Epidemiology. *Antibiotics* **12**, (2023).
18. Gayle M. Boxx, G. Cheng, The Roles of Type I Interferon in Bacterial Infection. *Cell Host & Microbe* **19**, 760–769 (2016).
19. X. Liu *et al.*, Activation of the JAK/STAT-1 Signaling Pathway by IFN-γ Can Down-Regulate Functional Expression of the MHC Class I-Related Neonatal Fc Receptor for IgG. *The Journal of Immunology* **181**, 449–463 (2008).
20. V. Szijártó *et al.*, Bactericidal Monoclonal Antibodies Specific to the Lipopolysaccharide O Antigen from Multidrug-Resistant Escherichia coli Clone ST131-O25b:H4 Elicit Protection in Mice. *Antimicrobial Agents and Chemotherapy* **59**, 3109–3116 (2015).
21. M. Shankar-Hari *et al.*, Endogenous IgG hypogammaglobulinaemia in critically ill adults with sepsis: systematic review and meta-analysis. *Intensive Care Medicine* **41**, 1393–1401 (2015).
22. D. C. Roopenian, S. Akilesh, FcRn: the neonatal Fc receptor comes of age. *Nature Reviews Immunology* **7**, 715–725 (2007).
23. S.-h. S. Lee, Phyllis. Gordon, Siamon. , Quantitative analysis of total macrophage content in adult mouse tissues. Immunochemical studies with monoclonal antibody F4/80. *The Journal of experimental medicine* **161**, 475–489 (1985).
24. D. K. Challa *et al.*, Neonatal Fc receptor expression in macrophages is indispensable for IgG homeostasis. *mAbs* **11**, 848–860 (2019).
25. X. Zhao *et al.*, Human Neonatal Fc Receptor Is the Cellular Uncoating Receptor for Enterovirus B. *Cell* **177**, 1553–1565.e1516 (2019).
26. F. Li *et al.*, Establishment of disseminated neonatal echovirus 11 infection model in hFcRn transgenic mice. *Virology Journal* **22**, (2025).

27. K. Haga *et al.*, Neonatal Fc receptor is a functional receptor for classical human astrovirus. *Genes to Cells* **29**, 983–1001 (2024).
28. X. Liu *et al.*, Human cytomegalovirus evades antibody-mediated immunity through endoplasmic reticulum-associated degradation of the FcRn receptor. *Nature Communications* **10**, (2019).
29. S. Qian *et al.*, Downregulation of FcRn promotes ferroptosis in herpes simplex virus-1-induced lung injury. *Cellular and Molecular Life Sciences* **82**, (2025).
30. R. B. Cejas, D. C. Ferguson, A. Quiñones-Lombraña, J. E. Bard, J. G. Blanco, Contribution of DNA methylation to the expression of FCGRT in human liver and myocardium. *Scientific Reports* **9**, (2019).
31. M. Cecconi, L. Evans, M. Levy, A. Rhodes, Sepsis and septic shock. *The Lancet* **392**, 75–87 (2018).
32. D. C. Angus *et al.*, E5 murine monoclonal antiendotoxin antibody in gram-negative sepsis: a randomized controlled trial. *Jama* **283**, 1723–1730 (2000).
33. K. Reinhart *et al.*, CD14 receptor occupancy in severe sepsis: Results of a phase I clinical trial with a recombinant chimeric CD14 monoclonal antibody (IC14)*. *Critical Care Medicine* **32**, 1100–1108 (2004).
34. M. L. Harrison *et al.*, Tumor Necrosis Factor α As a New Target for Renal Cell Carcinoma: Two Sequential Phase II Trials of Infliximab at Standard and High Dose. *Journal of Clinical Oncology* **25**, 4542–4549 (2007).
35. M. W. McCarthy, C. Chong, N. C. Riedemann, R. Guo, A Targeted Blockade of Terminal C5a Is Critical to Management of Sepsis and Acute Respiratory Distress Syndrome: The Mechanism of Action of Vilobelimab. *International Journal of Molecular Sciences* **26**, (2025).
36. E. Briassouli, N. Syrimi, S. Ilia, Hyperferritinemia and Macrophage Activation Syndrome in Septic Shock: Recent Advances with a Pediatric Focus (2020–2025). *Children* **12**, (2025).
37. A. P. J. Vlaar *et al.*, Anti-C5a antibody IFX-1 (vilobelimab) treatment versus best supportive care for patients with severe COVID-19 (PANAMO): an exploratory, open-label, phase 2 randomised controlled trial. *The Lancet Rheumatology* **2**, e764–e773 (2020).
38. R. S. Hotchkiss, G. Monneret, D. Payen, Immunosuppression in sepsis: a novel understanding of the disorder and a new therapeutic approach. *The Lancet Infectious Diseases* **13**, 260–268 (2013).
39. E. J. Giamarellos-Bourboulis *et al.*, The pathophysiology of sepsis and precision-medicine-based immunotherapy. *Nature Immunology* **25**, 19–28 (2024).
40. N. Gong *et al.*, Mannich reaction-based combinatorial libraries identify antioxidant ionizable lipids for mRNA delivery with reduced immunogenicity. *Nature Biomedical Engineering*, (2025).
41. X. Guan *et al.*, Engineered M2 macrophage-derived exosomes: mechanisms and therapeutic potential in inflammation regulation and regenerative medicine. *Acta Biomaterialia* **203**, 38–58 (2025).
42. H. Zhang, D. Liu, K. Yang, Z. Liang, M. Li, Ionizable guanidine-based lipid nanoparticle for targeted mRNA delivery and cancer immunotherapy. *Science Advances* **11**, eadx5970 (2025).

Acknowledgments: We thank the Biosafety Level 2 (BSL-2) and Animal Biosafety Level 2 (ABSL-2) Laboratories of the Institute of Infectious Diseases, Shenzhen Bay Laboratory, for their support and assistance during this research.

Funding:

National Natural Science Foundation of China: 32571106 (X.C.)

National Natural Science Foundation of China: 82371836 (X.C.)

Guangdong Pearl River Funding: 2023QN10Y181 (X.C.)

Start-up funding from Shenzhen Bay Laboratory (X.C.)

National Natural Science Foundation of China: 82501943 (W.C)

GuangDong Basic and Applied Basic Research Foundation: 2023A1515111092 (W.C)

Author contributions:

Conceptualization: X.C., X.W., X.S., and Q.D.

Methodology: X.W., X.S., M.P., Q.D., Q.H., X.L., J.Z., D.W., B.C., Y.D., Y.H., J.Y., and T.Z.

Validation: X.C., X.W., X.S., and Q.D.

Investigation: X.S. and X.W.

Resources: W.C., X.L., H.Z., X.H., M.L., and X.D.

Visualization: X.C., X.W., X.S., and Q.D.

Funding acquisition: X.C., and W.C.

Project administration: X.C., W.C., and X.L.

Supervision: X.C.

Writing – original draft: X.C., X.W., and X.S.

Writing – review & editing: X.C., W.C., and X.L.

Competing interests: Authors declare that they have no competing interests.

Data and materials availability: The raw sequence data reported in this paper have been deposited in the Genome Sequence Archive (Genomics, Proteomics & Bioinformatics 2025) in National Genomics Data Center (Nucleic Acids Res 2025), China National Center for Bioinformation / Beijing Institute of Genomics, Chinese Academy of Sciences (GSA: CRA036603) that are publicly accessible at https://ngdc.cncb.ac.cn/gsa.

Supplementary Materials

Materials and Methods

Figs. S1 to S7

References (*43–53*)

Fig. 1. Bacterial sepsis drives the loss of both endogenous and exogenous IgG. (**A**) Relative abundance of serum IgG in bacterial sepsis patients (survivors vs. non-survivors, n = 7 per group) over time. (**B** and **C**) Serum kinetics of total mIgG (B, *n* = 5) and mIgM (C, *n* = 10) in C57BL/6J mice with sepsis induced by pathogenic *E. coli* (1×10^8 CFU/mouse) or *S. aureus* Δ*spa*Δ*sbi*Δ*ssl10* (1×10^7 CFU/mouse), respectively. These inocula were used unless otherwise specified. (**D** and **E**) Serum hIgG (D) and hIgM (E) kinetics in IVIG (500 μg/mouse)-treated C57BL/6J mice (*n* = 5) during sepsis induced by pathogenic *E. coli* or *S. aureus* Δ*spa*Δ*sbi*Δ*ssl10*. (**F**) Serum hIgG1 kinetics in C57BL/6J mice (*n* = 5) following its administration and subsequent septic challenge with pathogenic *E. coli* or *S. aureus* Δ*spa*Δ*sbi*Δ*ssl10*. A dose of 100 μg mAb per mouse was used throughout (unless specified). (**G** and **H**) Serum hIgG1 kinetics in IgD & IgM double knockout C57BL/6J mice (*n* = 10) following its administration and subsequent septic challenge with pathogenic *E. coli* (G) or *S. aureus* Δ*spa*Δ*sbi*Δ*ssl10* (H). (**I**) Serum hIgG1^{YTE} kinetics in humanized FcRn C57BL/6N mice (*n* = 10) following its administration and subsequent septic challenge with pathogenic *E. coli*. (**J** and **K**) Serum kinetics of mIgG2b (J) or mIgM (K) mAb in C57BL/6J mice (*n* = 4 and 8) following its administration and subsequent septic challenge with pathogenic *E. coli*. (**L** and **M**) Concentration of exogenous hIgG1 in perfused (L) and non-perfused (M) murine tissues (*n* = 3 to 5) at 12 and 48 hours after septic challenge. (**N**) Relative levels of exogenous hIgG1 in murine feces (*n* = 5) at different times after septic challenge. Data are presented as mean ± SEM. Significant differences (*p < 0.05, **p < 0.01, and ***p < 0.001) were identified in B-D and F-J by two-tailed Student's *t* test.

Fig. 2. Loss of macrophage FcRn mediates circulating IgG loss in septic mice. (**A** and **B**) Flow cytometric analysis of relative FcRn expression in macrophages, monocytes, and endothelial cells from murine tissues (*n* = 3 to 5) at indicated times after septic challenge with *E. coli* (A) or *S. aureus* Δ*spa*Δ*sbi*Δ*ssl10* (B). (**C** and **D**) Flow cytometric (C, *n* = 3) and qPCR (D, *n* = 6 to 9) analysis of relative FcRn expression in bone marrow-derived macrophages (BMDMs) after *E. coli* (MOI 1) or *S. aureus* Δ*spa*Δ*sbi*Δ*ssl10* (MOI 5) infection. (**E**) Serum total mIgG kinetics in *Fcgrt*$^{-/-}$ C57BL/6J mice (*n* = 6) with *E. coli*-induced sepsis. (**F**) Serum hIgG1 kinetics in *Fcgrt*$^{-/-}$ C57BL/6J mice (*n* = 5 to 8) following its administration and subsequent septic challenge with *E. coli* or *S. aureus* Δ*spa*Δ*sbi*Δ*ssl10*. (**G**) Relative body weight in *Fcgrt*$^{f/f}$ and *Fcgrt*$^{f/f}$ *LysM-Cre* C57BL/6J mice (*n* = 6) with pathogenic *E. coli*-induced sepsis. (**H** and **I**) Bacterial loads in tissues from *Fcgrt*$^{f/f}$ and *Fcgrt*$^{f/f}$ *LysM-Cre* C57BL/6J mice (*n* = 5 to 7) at 96 hours after septic challenge with *E. coli* (H) or *S. aureus* Δ*spa*Δ*sbi*Δ*ssl10* (I). (**J** and **K**) Serum hIgG1 kinetics in *Fcgrt*$^{f/f}$ and *Fcgrt*$^{f/f}$ *LysM-Cre* C57BL/6J mice (*n* = 6 to 12) following its administration and subsequent septic challenge with *E. coli* (J) or *S. aureus* Δ*spa*Δ*sbi*Δ*ssl10* (K). Data are presented as mean ± SEM. Significant differences (*p < 0.05, **p < 0.01, and ***p < 0.001) were identified in A, B, J, and K by two-tailed Student's *t* test and in C and D by one-way ANOVA analysis.

Fig. 3. Bacterial LPS and PGN induce FcRn downregulation and IgG loss in mice. (**A**) Serum hIgG1 kinetics in *TLR4*$^{+/+}$ and *TLR4*$^{-/-}$ C57BL/6J mice (*n* = 5) following its administration and subsequent septic challenge with *E. coli*. (**B**) Serum total mIgG kinetics in C57BL/6J mice (*n* = 5) with *Acinetobacter baumannii* wild-type- or Δ*lpxC*-induced sepsis. (**C**) Serum hIgG1 kinetics in C57BL/6J mice (*n* = 5) following its administration and subsequent septic challenge with *Acinetobacter baumannii* wild-type (2×10^8 CFU/mouse) or Δ*lpxC* (6×10^8 CFU/mouse). (**D**) Serum hIgG1 kinetics in C57BL/6J mice (*n* = 11 to 15) following its administration and subsequent challenge with LPS (5 mg/kg) or PGN (10 mg/kg). (**E**) Serum total mIgG kinetics in

C57BL/6J mice (n = 17) with LPS (5 mg/kg) challenge. (**F**) Serum hIgG1^{YTE} kinetics in humanized FcRn C57BL/6N mice (n = 4) following its administration and subsequent LPS (5 mg/kg) challenge. (**G**) Serum hIgG1 kinetics in *TLR4*$^{-/-}$ mice (n = 8) following its administration and subsequent LPS (5 mg/kg) challenge. (**H** and **I**) Flow cytometric analysis of relative FcRn expression in macrophages isolated from murine tissues at indicated times after LPS (H, 5 mg/kg, n = 4) or PGN (I, 10 mg/kg, n = 3) challenge. (**J** and **K**) Flow cytometric analysis of relative FcRn expression in BMDMs (n = 3 to 5) after challenge with LPS (J) or PGN (K) at indicated times and doses. (**L**) Phagocytic analysis of FITC-dextran uptake by LPS-treated BMDMs (n = 6) from WT and *Fcgrt*$^{-/-}$ mice. (**M**) Determination of hIgG1 (Alexa Fluor 647-labeled) in LPS-treated BMDMs (n = 3) from WT and *Fcgrt*$^{-/-}$ mice by flow cytometry. (**N**) Determination of hIgG1 (Alexa Fluor 647-labeled) in PGN-treated BMDMs (n = 3) from WT mice by flow cytometry. (**O** and **P**) Serum hIgG1 kinetics in *Fcgrt*$^{-/-}$ C57BL/6J mice (n = 11 to 15) following its administration and subsequent challenge with LPS (M, 5 mg/kg) or PGN (N**,** 10 mg/kg). Data are presented as mean ± SEM. Significant differences (*p < 0.05, **p < 0.01, and ***p < 0.001) were identified in A to F, H, I, and N by two-tailed Student's t test and in J, K, and M by one-way ANOVA analysis.

Fig. 4. STAT1 activation mediates macrophage FcRn reduction and IgG loss in septic mice. (**A**) Effect of NF-κB inhibitor BAY11-7082 (BAY11, 10 μM) on *Fcgrt* expression in BMDMs (n = 6) treated with LPS (1 μg/ml) or PGN (10 μg/ml) for 12h. (**B**) qPCR analysis of *Fcgrt* expression in A129 mouse-derived BMDMs (n = 6) treated with LPS (1 μg/ml) for 12h. (**C** and **D**) Serum hIgG1 kinetics in A129 mice (n = 5) following its administration and subsequent challenge with *E. coli* (C) or LPS (D**,** 5 mg/kg). **(E)** Principal component analysis (PCA) of transcriptomic data from kupffer cells (KCs) and splenic macrophages (Macs) of septic mice induced by pathogenic *E. coli* or *S. aureus* Δ*spa*Δ*sbi*Δ*ssl10*. **(F)** Heat-map of shared sepsis-induced differentially expressed genes (DEGs) in kupffer cells and splenic macrophages. **(G)** Transcription factor (TF) activity inferred from shared DEGs. KC, Kupffer cell; SpMac: splenic macrophages. **(H)** Venn diagram showing the overlap between *Fcgrt*-regulating TFs identified from the macrophage cistrome and functionally inferred TFs from the shared DEGs. (**I**) qPCR analysis of *Fcgrt* expression in BMDMs (n = 5 to 27) treated with STAT1 inhibitor Fludarabine (50 μM) and stimulated with LPS (1 μg/ml) or PGN (10 μg/ml) for 12 h. (**J**) Western blotting analysis of STAT1 phosphorylation in BMDMs treated with *E. coli* (MOI 1) or *S. aureus* Δ*spa*Δ*sbi*Δ*ssl10* (MOI 5). β-actin was used as the loading control. (**K** to **N**) Flow cytometric analysis of relative FcRn expression in liver (K, L) and splenic (M, N) macrophages isolated from *Stat1*$^{-/-}$ mice and their controls (n = 3 to 5) at 24 hours after septic challenge with *E. coli* (K, M) or *S. aureus* Δ*spa*Δ*sbi*Δ*ssl10* (L, N). (**O** and **P**) Serum hIgG1 kinetics in *Stat1*$^{+/-}$ and *Stat1*$^{-/-}$ mice (n = 10) following its administration and subsequent septic challenge with pathogenic *E. coli* (O) or *S. aureus* Δ*spa*Δ*sbi*Δ*ssl10* (P). Data are presented as mean ± SEM. Significant differences (*p < 0.05, **p < 0.01, and ***p < 0.001) were identified in A, I, K, L, M, and N by two-way ANOVA analysis, in B, C, D, O, and P by two-tailed Student's t test, and in I by one-way ANOVA analysis.

Fig. 5. FcRn reduction and resultant IgG loss driven by PAMP-STAT1-FcRn axis are conserved in humans. (**A**) Analysis of *Fcgrt* expression in a public dataset (GSE65682) of whole-blood leukocytes from healthy donors and septic patients. (**B**) Assessment of survival probability of septic patients with low vs. high *Fcgrt* expression levels by analyzing the GSE65682 dataset. (**C**) Analysis of *Fcgrt* expression in a public dataset (GSE63042) of whole blood from bacterial sepsis survivors (n = 78) and non-survivors (n = 28). (**D**) Proportion

assessment of bacterial sepsis survivors (n = 78) and non-survivors (n = 28) with low or high *Fcgrt* expression by analyzing the GSE63042 dataset. (**E**) Flow cytometric analysis of FcRn expression in $CD14^+$ monocytes isolated from healthy donors (n = 35) and patients with bacterial sepsis (n = 22). (**F** to **I**) Flow cytometric analysis of FcRn expression in $CD14^+$ monocyte-derived macrophages (hMDMs, n = 3) at indicated times after challenge with *E. coli* (F**,** MOI 1), *S. aureus* Δ*spa*Δ*sbi*Δ*ssl10* (G, MOI 5), LPS (H**,** 1 μg/ml) or PGN (I, 10 μg/ml). (**J** and **K**) Western blotting analysis of STAT1 phosphorylation in hMDMs treated with *E. coli* (J**,** MOI 1), *S. aureus* Δ*spa*Δ*sbi*Δ*ssl10* (J**,** MOI 5), LPS (K**,** 1 μg/ml), or PGN (K**,** 10 μg/ml). β-actin was used as the loading control. (**L** and **M**) Flow cytometric analysis of relative FcRn expression in hMDMs pretreated with STAT1 phosphorylation inhibitors RUX (Ruxolitinib, targeting Tyr701) or ADE (Adezmapimod, targeting Ser727) and stimulated with LPS (L, n = 10) or PGN (M, n = 6) for 24 h. (**N**) Phagocytic analysis of FITC-dextran uptake by LPS- or PGN-treated hMDMs (n = 3). (**O**) Determination of hIgG1 (Alexa Fluor 647-labeled) in LPS- or PGN-treated hMDMs (n = 3). Data are presented as mean ± SEM. Significant differences (*p < 0.05, **p < 0.01, and ***p < 0.001) were identified in A, C, and E by two-tailed Student's t test, in B by the Kaplan-Meier survival analysis with the log-rank test, and in F, G, H, I, L, M and O by two-way ANOVA analysis.

Fig. 6. Antibody efficacy in bacterial sepsis is rescued by targeting PAMP-STAT1-FcRn axis. (**A** and **B**) Survival of $Fcgrt^{f/f}$ and $Fcgrt^{f/f}$ *LysM-Cre* C57BL/6J mice (n = 8 to 10) treated with PBS or IVIG following sepsis induced by *E. coli* (A, 3×10^8 CFU/mouse) or *S. aureus* Δ*spa*Δ*sbi*Δ*ssl10* (B, 5×10^7 CFU/mouse). IVIG was administered at 600 μg for *E. coli* and 900 μg for *S. aureus* challenges. These bacterial inocula and IVIG doses were used consistently unless stated otherwise. (**C** and **D**) Survival of $STAT1^{+/-}$ and $STAT1^{-/-}$ C57BL/6J mice (n = 9 to 15) treated with PBS or IVIG following sepsis induced by *E. coli* **(C)** or *S. aureus* Δ*spa*Δ*sbi*Δ*ssl10* **(D)**. (**E**) Survival of ICR (n = 10) mice pretreated with PBS or IVIG followed by carnosic acid (CA) prior to sepsis induction with *S. aureus* Δ*spa*Δ*sbi*Δ*ssl10*. (**F**) Survival of $TLR4^{+/+}$ and $TLR4^{-/-}$ C57BL/6J mice (n = 10) treated with hIgG1 or 3E9 following sepsis induced by *E. coli*. hIgG1 and 3E9 were administrated at a dose of 200 μg per mouse. (**G**) Serum 3E9 kinetics in $TLR4^{+/+}$ and $TLR4^{-/-}$ C57BL/6J mice (n = 5) following its administration and subsequent septic challenge with *E. coli*. **(H)** Survival of $Fcgrt^{f/f}$ and $Fcgrt^{f/f}$ *LysM-Cre* C57BL/6J mice (n = 8 to 9) treated with hIgG1 or 3E9 following sepsis induced by *E. coli*. hIgG1 and 3E9 were administrated at a dose of 500 μg per mouse. (**I**) Survival of $STAT1^{+/-}$ and $STAT1^{-/-}$ C57BL/6J mice (n = 8 to 10) treated with hIgG1 or 3E9 following sepsis induced by *E. coli*. hIgG1 and 3E9 were administrated at a dose of 200 μg per mouse. Data are presented as mean ± SEM. Significant differences (*p < 0.05, **p < 0.01, and ***p < 0.001) were identified in A-F, H, and I by the Kaplan-Meier survival analysis with the log-rank test and in G by two-tailed Student's t test.

Fig. 1.

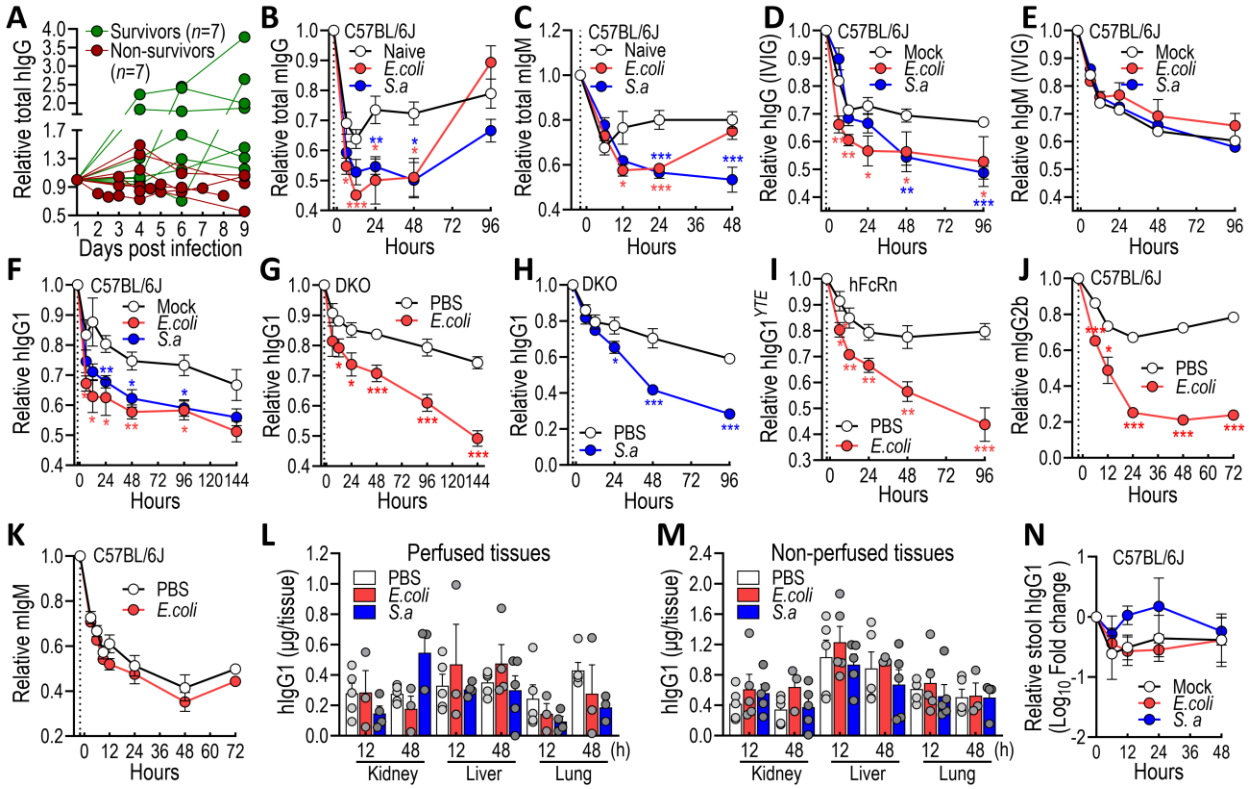

Fig. 2.

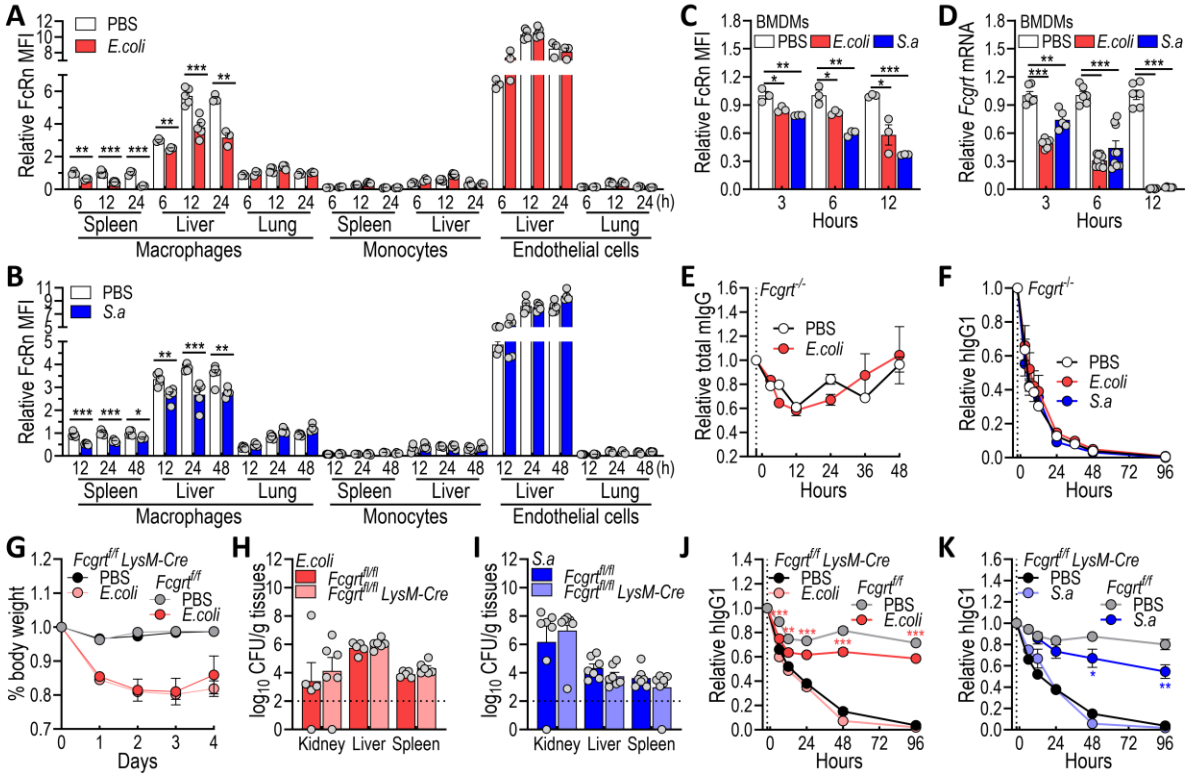

Fig. 3.

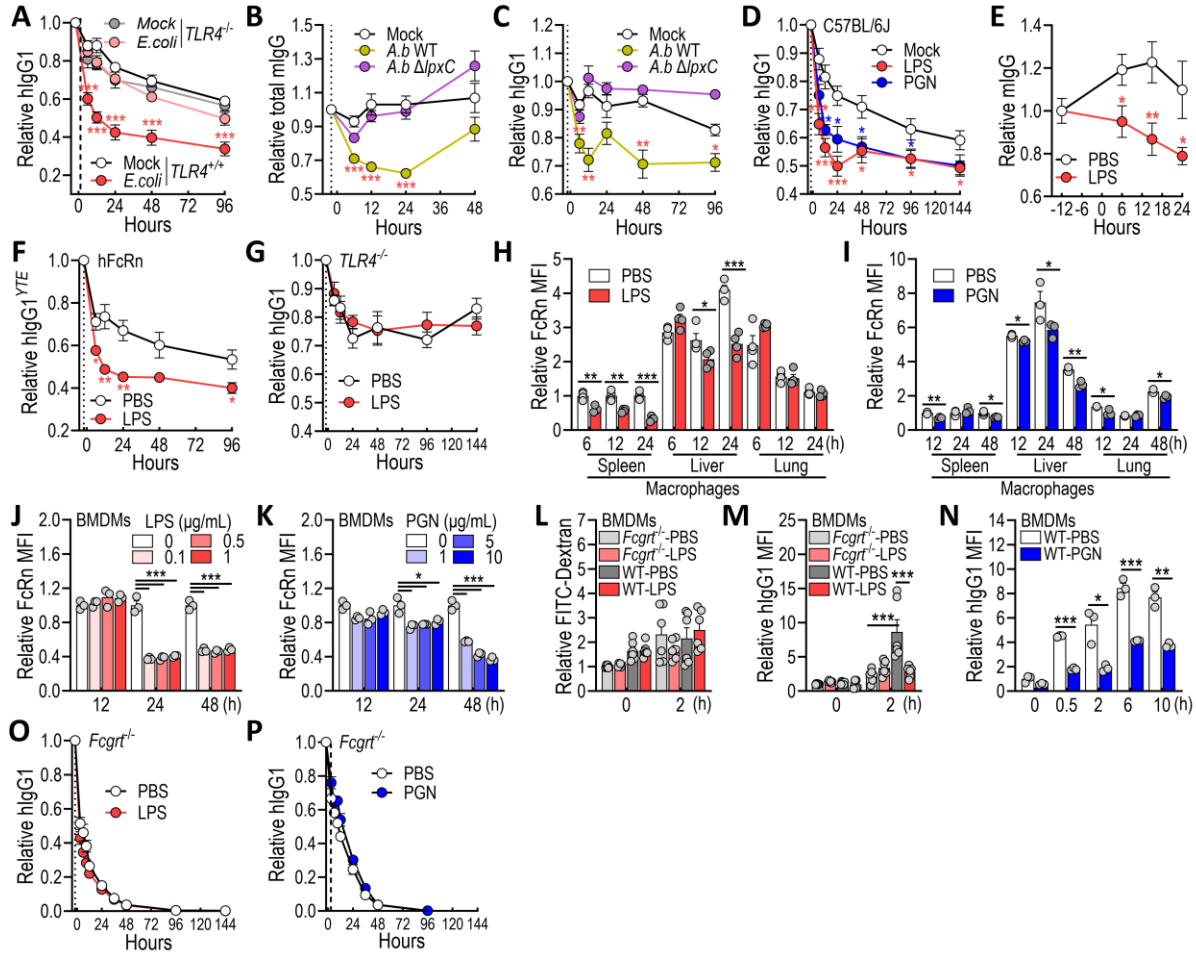

Fig. 4.

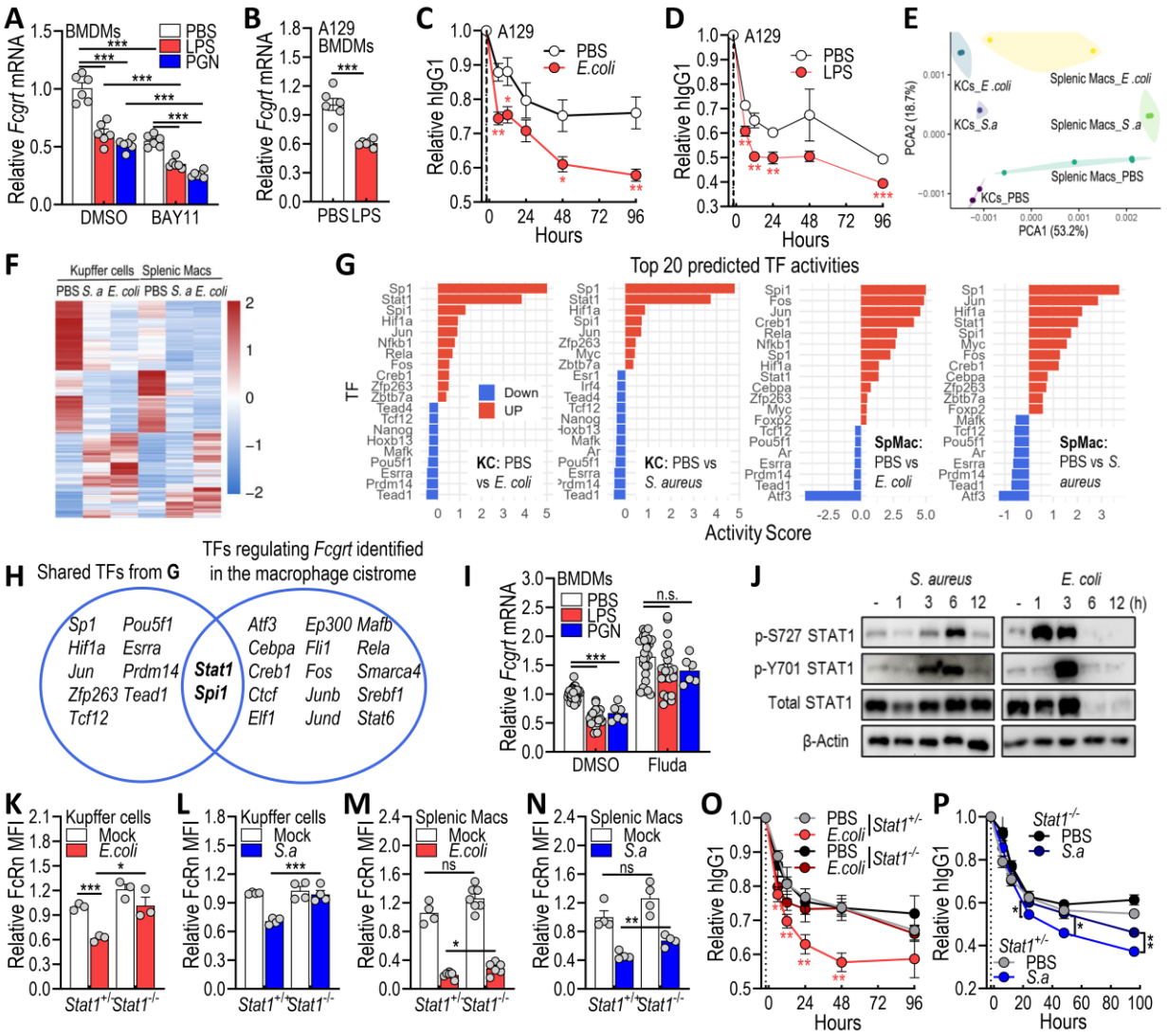

Fig. 5.

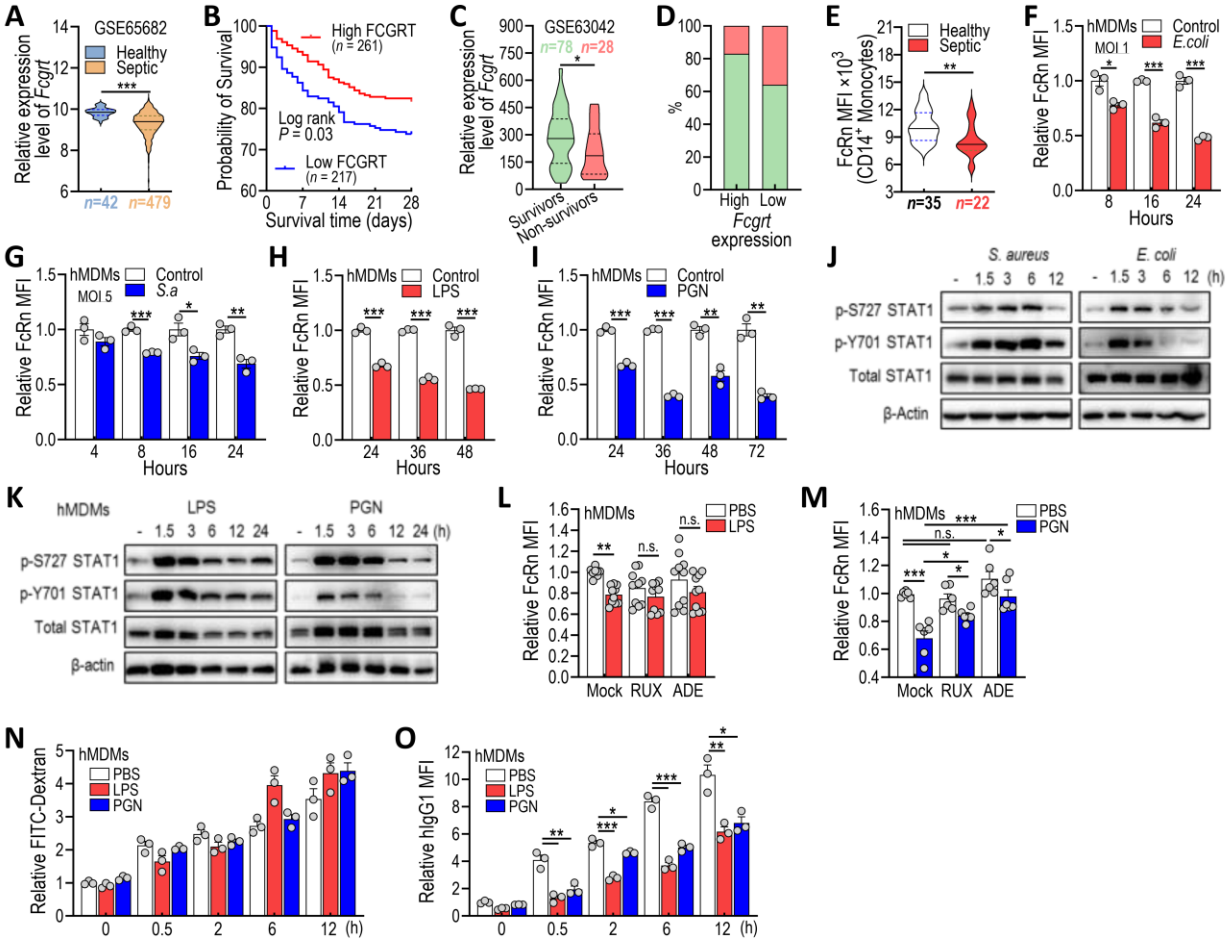

Fig. 6.